Needle-Based Interventions With the Image-Guided Surgery Toolkit (IGSTK): From Phantoms to Clinical Trials

Ziv Yaniv*, *Member, IEEE*, Patrick Cheng, Emmanuel Wilson, Teo Popa, David Lindisch, Enrique Campos-Nanez, Hernan Abeledo, Vance Watson, Kevin Cleary, *Member, IEEE*, and Filip Banovac

***Abstract*—We present three image-guided navigation systems developed for needle-based interventional radiology procedures, using the open source image-guided surgery toolkit (IGSTK). The clinical procedures we address are vertebroplasty, RF ablation of large lung tumors, and lung biopsy. In vertebroplasty, our system replaces the use of fluoroscopy, reducing radiation exposure to patient and physician. We evaluate this system using a custom phantom and compare the results obtained by a medical student, an interventional radiology fellow, and an attending physician. In RF ablation of large lung tumors, our system provides an automated interventional plan that minimizes damage to healthy tissue and avoids critical structures, in addition to accurate guidance of multiple electrode insertions. We evaluate the system's performance using an animal model. Finally, in the lung biopsy procedure, our system replaces the use of computed tomographic (CT) fluoroscopy, reducing radiation exposure to patient and physician, while at the same time enabling oblique trajectories which are considered challenging under CT fluoroscopy. This system is currently being used in an ongoing clinical trial at Georgetown University Hospital and was used in three cases.**

***Index Terms*—Computed tomography (CT), cone-beam computed tomography (CBCT), electromagnetic tracking, image-guided surgery, interventional radiology.**

I. Introduction

MOTIVATED by less trauma to the patient and lower overall costs, traditional open surgery is being replaced with minimally invasive techniques for many procedures. Most notably, this transition is characterized by the replacement of direct visual feedback with the use of images, resulting in an extended learning period.

In open surgery, the physician directly sees and feels the anatomical structures. In image-guided procedures, the physician mentally recreates the spatial relationship between tools and anatomy based on images, which are most often 2-D. As a result, the outcome is highly dependent upon the physician's ability to mentally reconstruct a 3-D scene from one or more two dimensional images.

Image-guided navigation systems aim at augmenting and complementing the physician's ability to understand the spatial structure of the anatomy by integrating medical images and other sources of information, such as tracked instruments. These systems potentially have a threefold effect: 1) they can shorten the learning period required for minimally invasive procedures and reduce the variability of the outcome, narrowing the gap between exceptional and standard practice; 2) they may enable new minimally invasive procedures, allowing physicians to perform procedures that were previously considered too dangerous; and 3) they transform qualitative procedure evaluations into quantitative ones, enabling a quantitative comparison between plan and execution.

The origins of image-guided navigation can be traced to the use of stereotactic frames in neurosurgical procedures. Since then, image-guided navigation systems have primarily been used in medical disciplines that deal with rigid anatomical structures, neurosurgery, and orthopedics. More recently, disciplines that deal with moving and deforming organs (e.g., interventional radiology) have started to utilize such systems [1].

In this paper, we describe three navigation systems developed for needle-based interventional radiology procedures, using the open source image-guided surgery toolkit (IGSTK) [2]. The IGSTK is a free open source C++ toolkit, providing a framework for rapid development of customized image-guidance applications. The toolkit provides a set of components common to most navigation systems. These include: 1) interfaces to various tracking devices; 2) Digital Imaging and Communications in Medicine (DICOM) image readers; 3) paired-point rigid body registration; and 4) visualization components. In addition, the toolkit includes an internal logging mechanism, which can be used both for debugging during program development and for documenting the clinical intervention, which can be replayed for educational purposes.

Manuscript received July 27, 2009; revised September 14, 2009. First published November 17, 2009; current version published March 24, 2010. This work was supported in part by the National Institutes of Health under Grant 1R01CA124377 (National Cancer Institute) and Grant 5R01EB007195 (National Institute of Biomedical Imaging and Bioengineering) and in part by the U.S. Army under Grant W81XWH-04-1-0078 and the Society of Interventional Radiology Dr. Ernest J. Ring Academic Development Grant. *Asterisk indicates corresponding author*.

*Z. Yaniv is with the Imaging Science and Information Systems Center, Department of Radiology, Georgetown University Medical Center, Washington, DC 20007 USA (e-mail: zivy@isis.georgetown.edu).

P. Cheng, E. Wilson, T. Popa, K. Cleary, and F. Banovac are with the Imaging Science and Information Systems Center, Department of Radiology, Georgetown University Medical Center, Washington, DC 20007 USA (e-mail: cheng@isis.georgetown.edu; wilsone@isis.georgetown.edu; popa@isis.georgetown.edu; cleary@isis.georgetown.edu; banovac@isis.georgetown.edu).

D. Lindisch is with the Department of Radiology, Veterans Affairs Medical Center, Washington, DC 20420 USA (e-mail: david.lindisch@va.gov).

E. Campos-Nanez and H. Abeledo are with the Department of Engineering Management and Systems Engineering, George Washington University, Washington, DC 20052 USA (e-mail: ecamposn@gwu.edu).

V. Watson is with the Department of Radiology, Georgetown University Hospital, Washington, DC 20007 USA.

Color versions of one or more of the figures in this paper are available online at http://ieeexplore.ieee.org.

Digital Object Identifier 10.1109/TBME.2009.2035688

Although all three navigation systems share a common foundation, each is tailored to a specific clinical procedure workflow. This approach is motivated by our observation that procedure workflow is one of the key factors influencing clinical acceptance of image-guided navigation systems [3]. The procedures we address are vertebroplasty, RF ablation (RFA) of large lung tumors, and lung biopsy.

The first procedure we address is vertebroplasty. This is a minimally invasive procedure in which bone cement is injected into a fractured vertebral body that has been weakened by osteoporosis, long-term steroid use, or cancer. The cement is injected through a trocar, large bore hollow needle, that is percutaneously inserted through the pedicle of the vertebral body. This is a difficult procedure to perform, as the physician is inserting the trocar through a narrow structure in close proximity to the spinal cord relying solely on 2-D X-ray projection images [4]. To reconstruct the underlying 3-D scene, the physician repeatedly acquires X-ray images. As a result, there is an increase in radiation exposure both to the patient and to the medical staff [5]–[7].

The second procedure we address is RFA of large lung tumors. This is a percutaneous procedure in which tissue is ablated by delivering energy via an RF electrode. The size and shape of the ablated spatial region is dependent upon the electrode structure and the tissue characteristics. The goal of the procedure is to cause cell death of the entire tumor and roughly a 1 cm margin surrounding the tumor. Currently, the largest possible ablation region using a single electrode has a diameter of between 4 and 5 cm [8]. As a result, the highest treatment success rates are obtained for tumors that have a diameter of less than 2 to 3 cm [9], [10]. For larger tumors recurrence at the edge of the ablation zone is common.

A possible solution is the use of multiple ablations in an overlapping manner as proposed for liver RFA [11], [12]. Two challenges are associated with this approach, planning an optimal treatment and executing it. The optimal treatment should result in an ablation plan that encompasses the tumor and margin while minimizing the risk of complications such as pneumothorax, introduction of air into the pleural cavity potentially resulting in a collapsed lung, and damage to critical structures in the vicinity of the tumor. Executing such a plan is challenging as it requires repeated accurate placement of the RF electrode.

The last procedure we address is lung biopsy performed under computed tomographic (CT) fluoroscopy. In this procedure a biopsy is acquired by percutaneously inserting a needle into the suspect lesion with CT fluoroscopy, serving as a real-time imaging modality. The primary challenge in this procedure is that the imaging modality only provides a single tomographic image. Oblique trajectories are thus hard to monitor as the needle and tumor are not simultaneously visible on the image plane. In addition, the physician and patient are exposed to ionizing radiation [13], [14].

The image-guided navigation systems we developed address the challenges presented by each of these procedures. In vertebroplasty, our system replaces the constant use of fluoroscopy with the use of a preoperative cone-beam CT (CBCT), enabling dynamic 3-D navigation during trocar insertion. In RFA of large lung tumors, our system provides an interventional plan that minimizes risk in addition to accurate guidance for multiple electrode insertions using a preoperative CBCT for guidance. Finally, the system we developed for lung biopsy replaces the continuous use of CT fluoroscopy with the use of a preoperative CT scan acquired at breath hold, enabling oblique trajectories with no intraoperative radiation exposure.

Recently introduced commercial navigation systems that address similar clinical procedures include the PercuNav system from Traxtal Inc., A Philips Healthcare Company (Toronto, Canada), and the iGuide CAPPA system from Siemens AG Healthcare (Erlangen, Germany). Both systems provide navigation guidance, using the Aurora electromagnetic tracking device from Northern Digital Inc. (Waterloo, ON, Canada). Planning in these systems is optional. To plan a trajectory, the user indicates a target and entry point on the 3-D image. Both systems provide automatic rigid registration without the need to digitize fiducials in patient space. Navigation guidance is then provided using reformatted slices of the 3-D image with the tracked tools overlayed onto the images. In addition, the PercuNav system can import and display intraoperative ultrasound, registered to the 3-D image, for real-time update of the underlying anatomical structures and instruments. For our procedures this capability is not relevant as we are dealing with the lung and vertebra.

Additional noncommercial systems intended for guidance of liver RFA have been presented by Mundeleer *et al.* [15], State *et al.* [16], and Nicolau *et al.* [17]. All three navigation systems use optical tracking devices. Of the three systems, only the first one provides an explicit interventional plan. The plan is obtained via optimization with the assumption that both tumor and ablations are spherical. All three systems perform registration using the rigid body assumption, with the third system providing automated fiducial-based registration. Navigation guidance in the first system is provided using iconic representations of the needle and target and a surface rendering of the segmented liver vessels and tumor. In the second system, guidance is provided using an augmented reality approach with surface rendering of the tumor overlayed onto real-time ultrasound data. Finally, the third system provides guidance using an augmented reality approach with 3-D renderings of the anatomy overlaid onto video images.

We next describe the common framework of our navigation systems and the specific details that are unique to each procedure.

II. Navigation Systems

The navigation systems described in this work were developed using components available in the IGSTK [2] with customized extensions supporting the different registration, planning, and workflow that are specific to each of the clinical procedures.

The 3-D imaging modality used for guidance is CT or CBCT, with procedures performed either in the interventional radiology suite or the CT suite. The primary differences between these two similar modalities is that CBCT has lower discrimination between tissue types and a smaller spatial extent than CT [18]. Use of MR data is also possible but is not commonly used for interventions in our clinical environment.

In all interventions, we use the Aurora electromagnetic tracking device. Instruments are tracked using embedded five degrees of freedom (5 DOF) sensors. These sensors report their pose up to an unknown rotation around the sensor axis. In our case, this is sufficient as the sensors are embedded into cylindrical tools with the sensor and tool axis coinciding. The offset between the sensor location and the tool tip is either given by the manufacturer or estimated using pivot calibration [19]. As electromagnetic tracking accuracy is susceptible to distortions caused by ferromagnetic materials found in the environment, we evaluated the Aurora in both clinical environments [20] in which we work. We observed that the tracking accuracy is sufficient for all procedures carried out in the interventional radiology suite, and that navigation in the CT suite should be performed away from the CT gantry.

We use the following time-line view to describe our systems functionality.

1) *Data acquisition*: Place fiducial markers and acquire preoperative 3-D images at breath hold.
2) *Planning*: Define one or more needle trajectories.
3) *Registration*: Use rigid paired-point registration to align the image coordinate system to the patient one.
4) *Navigation*: Provide visual feedback to the physician facilitating accurate execution of the plan.

It should be noted that the vertebroplasty and lung RFA systems perform these steps in this order, but that in the lung biopsy system part of the plan is specified prior to registration and part after registration.

The guidance during the navigation step is similar in all of our systems. It is based on a custom graphical user interface (GUI) tailored for needle insertion along a predetermined trajectory to a given target. The trajectory and target point are provided by the planning step, which is procedure specific.

Our GUI provides the physician with three reformatted views through the volumetric data: axial, off-axial, and off-sagittal or off-coronal. The off-axis views are reformatted planes that follow the needle axis. These are tilted axial, sagittal, and coronal views so that the needle shaft is visualized in plane. The planned trajectory is then displayed in all views alongside the dynamically updated needle location and reslice planes.

The use of off-axis views is based on current clinical practice for needle-based biopsies under interventional CT. In these procedures, the physician attempts to plan the needle insertion so that the needle shaft is in the fixed imaging plane. As we use a volumetric data set, we can tilt the standard image planes to the needle shaft.

The tilted views are obtained as follows. Given the needle shaft direction $\mathbf{u}$ and needle tip location $\mathbf{p}$, both defined in the image coordinate system, the off-axial reslice plane is defined as

$$\mathbf{n}^{\mathrm{T}}(\mathbf{q_i} - \mathbf{p}) = 0$$

where $\mathbf{n} = \mathbf{u} \times \mathbf{x}$, and the camera's up direction is given as $\mathbf{n} \times \mathbf{x}$. A point $\mathbf{q_i}$ is thus on the plane if it satisfies the equation mentioned earlier. Note that when $\mathbf{u} \times \mathbf{x} \simeq \mathbf{0}$, we set $\mathbf{n} \equiv \mathbf{z}$. The off-sagittal and off-coronal planes are obtained similarly. Fig. 1 illustrates this concept.

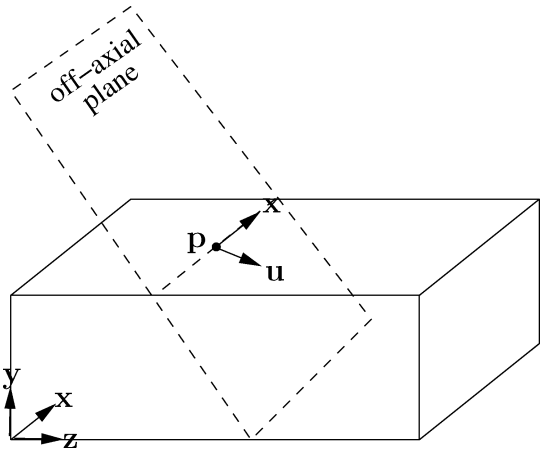

Fig. 1. Off-axis view, tilting the axial (*xy* plane) view so that the needle shaft is in the viewing plane. $\mathbf{u}$ is the needle shaft direction and $\mathbf{p}$ is the needle tip, both in the image coordinate system.

Finally, we provide a targeting view. The target is displayed as a sphere, the needle tip as a ring, and the needle hub as a wider ring. These are displayed on a plane defined using the point-normal plane parametrization

$$\mathbf{v}^{\mathrm{T}}(\mathbf{x_i} - \mathbf{p}) = 0$$

where $\mathbf{p}$ is the needle tip and $\mathbf{v}$ is the planned trajectory in the image coordinate system. Based on physician preference, we can also display the image corresponding to this reformatting plane. At the bottom of this window, we display the distance between the needle tip and the target point.

Inserting the needle to the target is done in three steps.

1) Move the needle tip on the skin surface till the ring representing the tip is centered on the target sphere. This is the entry point.
2) Pivot the needle at the entry point so that all three elements are centered. At this point the needle shaft and planned trajectory are aligned.
3) Advance the needle while watching the depth gauge that displays the distance between the needle tip and the target.

Fig. 2 shows a snapshot of the display from a clinical lung biopsy case.

We next describe in detail the system specific steps.

A. Vertebroplasty System

The vertebroplasty navigation system provides the physician with guidance during the percutaneous insertion of the trocar through the pedicle and into the vertebral body. Fig. 3 shows the system in use during a phantom study. The tracked tools were provided by Traxtal Technologies Inc. (Toronto ON, Canada) and included two 22 gauge MagTrax needles and a modified trocar, KyphX Osteo introducer with an embedded electromagnetic sensor.

The system follows the four-step workflow outlined earlier. We next describe each of these steps in detail.

1) Data acquisition: At our institute vertebroplasty is commonly performed in the interventional radiology suite. As our

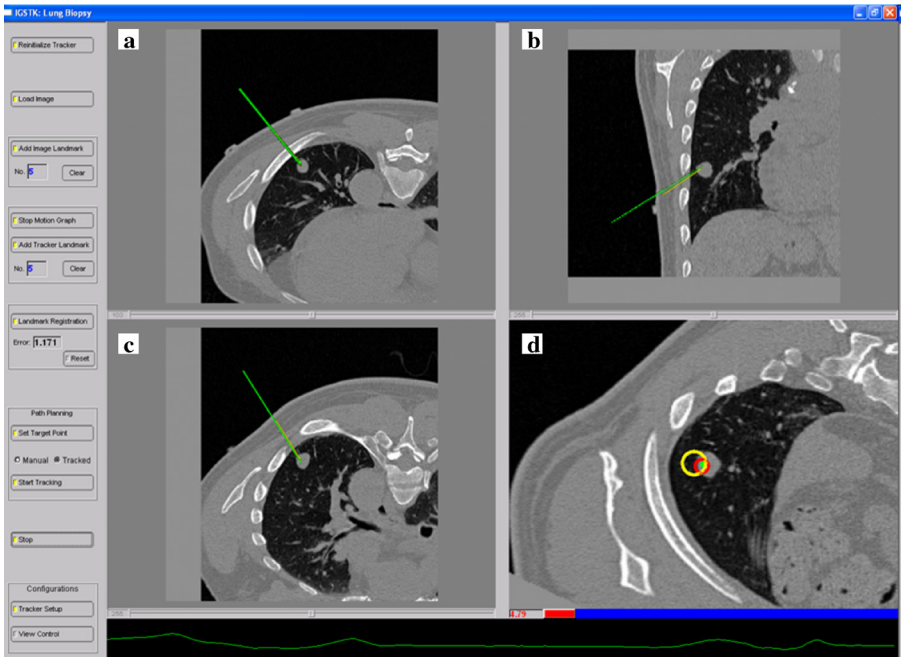

Fig. 2. Navigation GUI as shown during a clinical lung biopsy case: (a) axial view, slice closest to the needle tip; (b) off-coronal view; (c) off-axial view; (d) targeting view. Notice that in the axial view, the needle seems to intersect the rib, which is clearly not the case, as seen in the off-axial view.

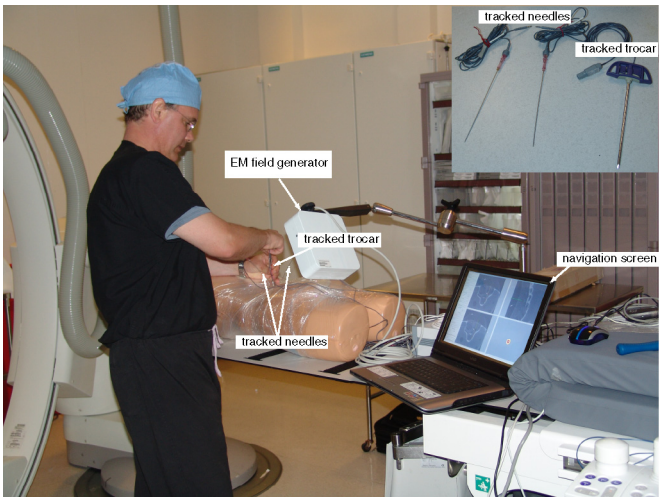

Fig. 3. Phantom study using vertebroplasty navigation system. Inset shows closeup of tracked needle fiducials and vertebroplasty trocar.

system provides guidance using 3-D images, we utilize a CBCT that is available *in situ*. In our case, this is the Axiom Artis dFA (Siemens AG Healthcare, Erlangen, Germany). The images we obtain are $256 \times 256 \times 221$ with a 0.8-mm isotropic spacing. The data is directly downloaded to a DICOM server running on the navigation system's computer.

Our fiducial markers are two 5 DOF, 22 gauge, electromagnetically tracked needles. The needles are inserted into the perispinal muscles lateral to the spinous process of the vertebra of interest. This is done percutaneously, with the patient in the prone position. Once the needles are firmly lodged they form a rigid body with the vertebra. This pair of needles serves a dual purpose. They are used as fiducials for registration, and after registration the two 5 DOF needles serve as a single 6-DOF dynamic reference frame, accounting for motion of the vertebral body.

Once the fiducials are placed, a CBCT scan is acquired and a plan is formulated.

2) Planning: To plan the intervention the 3-D image is displayed using the standard axial, sagittal, and coronal views. The physician scrolls through the image stack in each of the views and manually identifies a target point in the vertebral body and an entry point on the pedicle. These two points define a desired trajectory and target, which are displayed for approval. Once the plan is approved, we register the image and patient spaces.

Given the simplicity of the plan, a single trajectory, this step in the workflow could have been eliminated. We require that the physician explicitly provide a plan, such that, in case of failure, we can better identify the cause. In such cases, problems can be traced either to an erroneous plan or to problems executing a valid plan.

3) Registration: Image to patient registration is similar to the approach presented in [21]. It is based on the use of fiducials that provide both location and orientation information. As a result, we need only two fiducials to perform 3-D/3-D rigid registration.

We use two electromagnetically tracked needles as the fiducials. A tracked electromagnetic sensor coil is embedded in the needle's shaft approximately 10 mm from the tip, with the coil's main axis aligned with the needle's main axis. Thus, the needle's orientation can be read directly from the tracking device. The location of the needle tip relative to the embedded sensor is estimated using pivot calibration [19].

Once the needles have been inserted, and the CBCT data acquired, the physician manually identifies the needle tip and

a point on the needle shaft in the 3-D image. This defines the shaft direction in the image coordinate system. We then obtain a second, virtual fiducial, point on the needle shaft at a distance of 20 mm from the needle tip. This specific offset was chosen based on the physical characteristics of our needles. The needle is locally rigid with respect to the sensor coil. As our sensors are embedded approximately 10 mm from the needle tip, we defined our virtual point 10 mm in the opposite direction from the needle tip. This 20 mm region around the sensor coil does behave as a rigid body. Once the two needles are identified in the images, we have four points in the image coordinate system. The needle tip and shaft are localized in the 3-D image with a variability of less than 1.3 mm as previously assessed in [22].

We then position the electromagnetic field generator next to the patient and read the sensors' locations and orientations. Each needle provides us with two point locations in the patient coordinate system. These are the needle tip, obtained using the sensor location information and the pivot calibration, and the virtual fiducial point, obtained from the sensor location and orientation. Rigid registration is then computed automatically using these four points as input to a quaternion-based analytic pose estimation algorithm [23].

4) Navigation: Navigation is performed as described earlier. When the operator judges that the trocar is sufficiently close to the target, the navigation step ends and cement can be injected into the vertebral body.

B. Lung RFA System

The lung RFA procedure is performed in the interventional radiology suite, with the patient lying in the supine position. The interventional plan, set of trajectories and ablations, is computed by the system based on a manually specified segmentation. Guidance is then provided during the multiple needle insertions required for ablating large lung tumors.

During the navigation step the system utilizes an electromagnetically tracked needle consisting of a trocar, outer hollow part, and stylet, interchangeable inner bayonet-like part. Once the target has been reached the stylet is removed, the RFA electrode is inserted and the tissue is ablated. Fig. 4 shows the system used in an approved animal study. The tracked 18 gauge MagTrax needles were provided by Traxtal Technologies Inc. (Toronto, ON, Canada).

The system has the same four step workflow as the verbebroplasty system described earlier. We next describe each of the steps in detail.

1) Data acquisition: For this procedure we use the multimodality skin adhesive fiducials from IZI Medical Products Corp. (Baltimore, MD). At least four fiducials are placed on the thorax. In addition, we use an electromagnetically tracked needle inserted beneath the skin as an internal fiducial. The 3-D image is obtained using the same CBCT as used for vertebroplasty. To minimize reconstruction artifacts due to respiratory motion, the 3-D image is acquired using a breath hold approach at end expiration.

Once the fiducials are placed and the CBCT scan is performed, the system proceeds to the planning step.

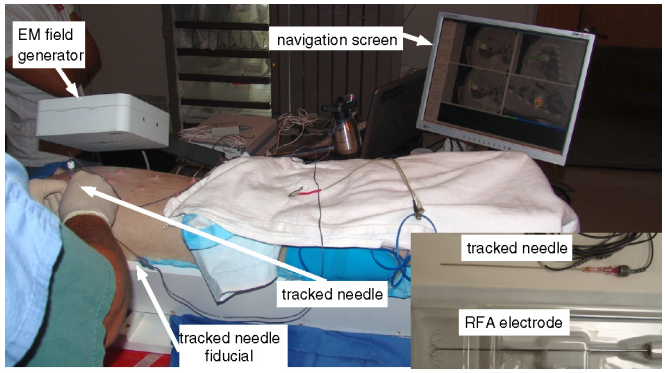

Fig. 4. Animal study using lung RFA navigation system. Inset shows closeup of hardware used in the procedure, tracked 18 gauge MagTrax needle (Traxtal Technologies Inc.), and clinical LeVeen CoAccess needle-electrode RFA system (Boston Scientific International).

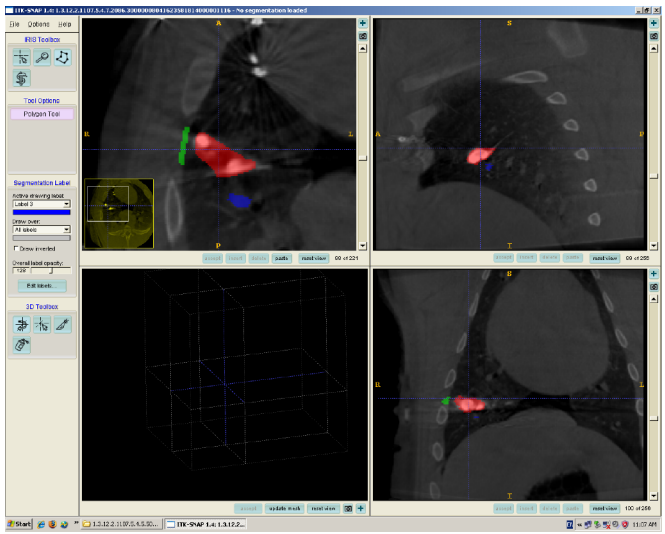

Fig. 5. Manual segmentation of classes used as input for RFA planning. Green (see electronic copy) denotes possible entry points, Red denotes tumor, and blue denotes structures that the needle should not traverse.

2) Planning: The system's planning step receives as input the effective ablation radius of the RFA electrode, and a manual segmentation of the 3-D image into the following classes:

1) tumor (T);
2) ablation margin (M);
3) potential needle entry points (E);
4) structures that the needle should not pierce (NP), such as ribs;
5) structures that should not be ablated (NA), such as the mediastinal structures.

Manual segmentation is performed using the ITK-SNAP Program [24], as shown in Fig. 5. The ablation margin class is automatically added based on the manually marked tumor. The physician specifies a desired ablation margin, and the tumor is dilated using a spherical structuring element having a radius corresponding to the desired ablation margin. Finally, the

segmentation is represented as a discrete point set, obtained by superimposing a lattice onto the segmented images.

Based on clinical considerations, the tumor and margin are ablated in addition to the following multiple optimization goals, given in rank order.

1) Minimize the number of punctures to the pleura, reduces the risk of pneumothorax.
2) Minimize the number of needle insertions through the same pleural entry point, reduces the risk of pneumothorax.
3) Minimize the number of ablations, minimizes the procedure duration.
4) Minimize damage to healthy tissue.

Given these goals and priorities, we employ a preemptive goal programming approach, where potential pleural entry points are analyzed one at a time, and the optimization goals are added incrementally. At each phase, we formulate the problem as an integer linear programming optimization and solve it using the branch and bound method. Our first objective is to determine the smallest set of needle trajectories needed to cover the lesion and its margin, given a particular pleural entry point. Once we obtain this set of trajectories, we determine the minimal number of ablations required for this set of trajectories. These two steps are repeated for all entry points. After all potential entry points have been analyzed, we choose the one that has the smallest number of needle trajectories and the least number of ablations, in that order. Finally, we employ a heuristic that minimizes the damage to healthy tissue, providing us with our optimal plan. The detailed formulation of our approach is presented in the Appendix.

3) Registration: Similar to the vertebroplasty system, we register image and patient spaces, using a 3-D/3-D analytic rigid registration method [23]. Each fiducial is manually localized in the 3-D image. The electromagnetic field generator is then placed next to the patient, and the fiducials are digitized using a tracked needle. As the image data were acquired at end expiration, the location of the digitizing needle is acquired at the same respiratory phase.

4) Navigation: Navigation is performed as described earlier, with one important difference. The operator only advances during the respiratory phase in which the 3-D image data were acquired. That is, the physician gates actions to end expiration. In all other respiratory phases, the image data are invalid. To perform the ablations, the physician first selects a trajectory and then navigates to each of the ablation locations along that trajectory. Once the operator judges that the tracked needle is sufficiently close to the ablation location its stylet is removed, the RFA electrode is inserted into the trocar and the tissue is ablated. This process is repeated for all planned ablation locations along the chosen trajectory and for all trajectories.

C. Lung Biopsy System

The lung biopsy procedure is performed in the CT suite. The navigation system provides physicians with an online planning mechanism, with the targeted lesion defined on the images before registration and the trajectory planned online during the intervention. Navigation is performed using an electromagnetically tracked needle consisting of a trocar and stylet. Once the target is reached, the stylet is retracted and a standard aspiration needle is used to obtain the biopsy. Fig. 6 shows the system in use in an approved clinical trial.

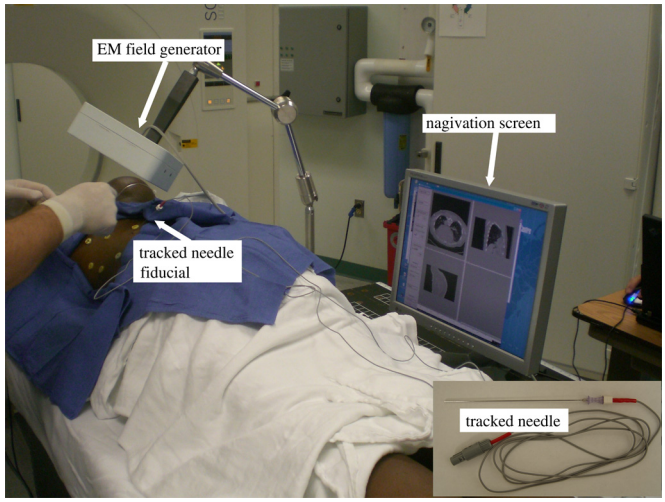

Fig. 6. Clinical trial using lung biopsy navigation system. Inset shows closeup of hardware used in the procedure, tracked 18-gauge needle (Amedo Smart Tracking Solutions GmbH).

1) Data acquisition: For this procedure, we use the same fiducial configuration as used in the lung RFA procedure, a number of skin adhesive fiducials and an electromagnetically tracked needle inserted beneath the skin. The 3-D image is acquired at breath hold, similar to the data acquisition performed in the lung RFA procedure. The only difference is that the imaging modality is CT instead of the C-arm-based CBCT.

Once the CT scan is acquired, the physician partially specifies the interventional plan.

2) Planning, target definition: Prior to registration the physician indicates the desired biopsy location on the image. Most often this is the center of the suspected lesion.

3) Registration: Registration is performed as described for the lung RFA system, with fiducials digitized at end expiration.

4) Planning, trajectory definition: Once the patient and image spaces are registered, the physician moves the tracked needle on the patient's skin. The trajectory defined by the needle tip and the pre-specified target is interactively displayed overlaid onto reformatted axial, sagittal and coronal slices. Once the physician is satisfied with a trajectory, it is fixed and the interventional plan is defined.

5) Navigation: Navigation is performed in the same gated manner as done when using the lung RFA system. In this case, there is a single trajectory instead of the multiple trajectories used by the lung RFA system. Once the physician judges that the tracked needle is sufficiently close to the biopsy location, the stylet is removed, the core biopsy needle is inserted through the trocar, and a sample is obtained. A validation scan can be readily acquired once the tracked needle is in place, ensuring that the sample is obtained from the desired location.

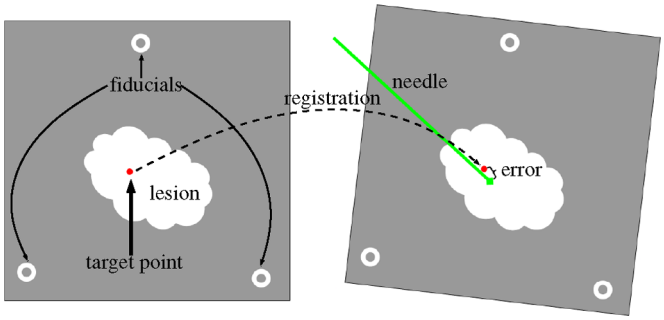

Fig. 7. Navigation accuracy analysis. Target point is transformed from the planning image, left, to the confirmation image, right. System accuracy is defined as the distance between the needle tip and the intended target on the confirmation image.

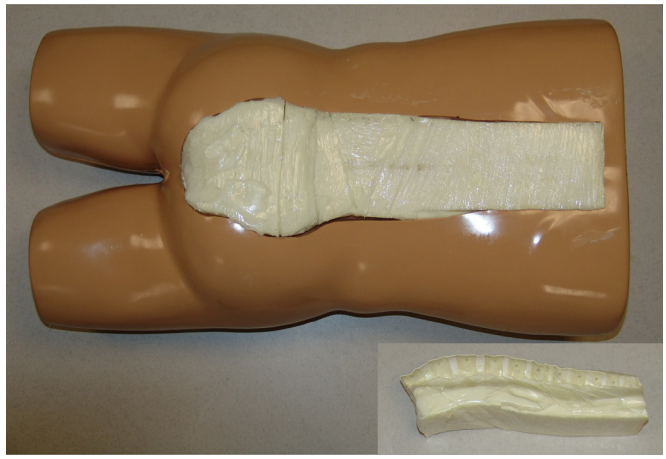

Fig. 8. Torso phantom used in vertebroplasty evaluation. Inset shows spinal column.

III. Experimental Evaluation

The vertebroplasty navigation system was evaluated using an anthropomorphic phantom. The lung RFA system was evaluated using an animal model, and the lung biopsy system was evaluated in an ongoing clinical trial at Georgetown University Hospital. The animal experiments were done with approval of the Georgetown animal care and use committee, and the human clinical trial was done under an approved Institutional Review Board protocol.

For all systems, navigation accuracy was assessed based on the distance between the needle tip and the intended target as they appear in a 3-D confirmation image, acquired after navigation. In the vertebroplasty system, this is a straightforward measurement as the system is evaluated using a phantom with easily identifiable targets, embedded ball bearings. In the lung RFA and lung biopsy systems, the targets are lesion points specified on the original 3-D image and cannot be easily identified in the validation image. To evaluate navigation accuracy using these systems, we perform an additional registration step.

The original 3-D image and the confirmation image are acquired at the same respiratory phase, end expiration. We can thus align the two images using rigid registration. Corresponding fiducial markers are identified in both images, and the target point location is transformed to the confirmation scan coordinate system. Fig. 7 visually illustrates this process.

To assess the validity of our quasi-rigid registration approach in the lung procedures, we use the fiducial registration error (FRE) [25]. While this measure is uncorrelated with the target registration error [26], it is useful for assessing the rigidity of the point configurations in image and patient spaces. In our case, a low FRE confirms that the digitized fiducials in patient space were acquired at the same respiratory phase as the 3-D image.

A. Vertebroplasty System

To evaluate the effectiveness of our system and the possibility that it can improve the performance of less experienced physicians, we performed the following phantom study. The vertebroplasty procedure was carried out by three operators having different levels of experience with the procedure, an attending interventional neuroradiologist, an interventional radiology fellow, and a medical student. Each participant performed the procedure ten times on an anthropomorphic spine phantom consisting of a torso and vertebral column (Sawbones worldwide, Pacific Research Laboratories Inc., Vashon, WA).

The phantom was modified for our purposes as follows. We embedded 2 mm steel ball bearings into the vertebral bodies in clinically viable locations so as to provide well-defined targets. We also fixed the spine in place using urethane foam. This was necessary as the fixation provided by the original phantom was insufficient, exhibiting considerable motion, approximately 10 mm, which is larger than that observed in practice. Fig. 8 shows this modified phantom.

Each participant performed ten trocar insertions into different vertebral bodies. After each insertion, a confirmation CBCT volume was acquired. For each attempt, we determined if the insertion was successful, the trocar was completely inside the pedicle. We also measured the distance between the trocar's tip and the target point and the time it took to complete the task.

Using our system, the participants successfully completed all trocar insertions. The mean (std) distance from the trocar tip to the target point for the attending was 1.90 (0.66) mm, for the fellow, it was 2.29 (1.26) mm, and for the medical student, it was 3.13 (1.38) mm. The mean (std) duration of the procedure for the attending was 99 (32) s, for the fellow, it was 178 (79) s, and for the student, it was 189 (67) s. Fig. 9 summarizes this study. The three levels of expertise are clearly reflected both in accuracy and procedure duration.

B. Lung RFA System

To evaluate our lung RFA system, we performed the following approved animal survival study. An attending interventional radiologist performed the lung RFA procedure, using our system to ablate simulated lung lesions in three swines. Simulated lesions were created by injecting a solution of agar, distilled water, and contrast material into the animal's lung, similar to the approach described in [27]. Once the procedure was completed, the animal was returned to the veterinary medicine facility for three days after which it was euthanized.

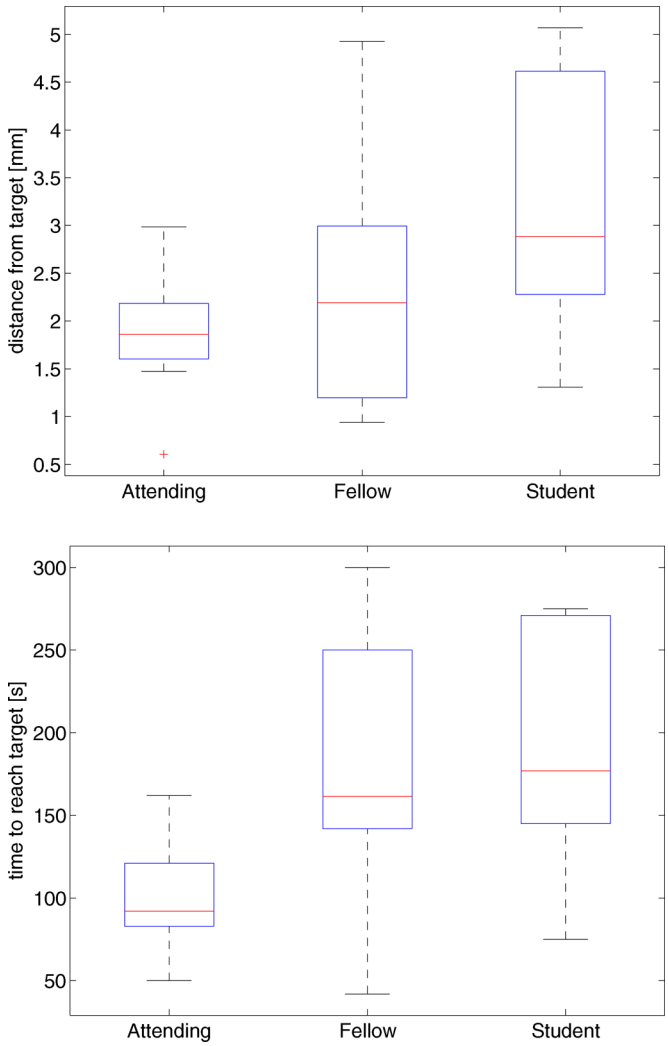

Fig. 9. System evaluation for three users with varying level of expertise accuracy (top), and procedure duration (bottom). The levels of expertise are clearly reflected both in execution accuracy and procedure duration. Standard values used in plot construction, box spans interquartile range, median marked inside box and maximal whisker length is set to 1.5 times interquartile range.

The first study was successful. Once the manual segmentation was completed, the automated plan was computed within 472 s, and consisted of two trajectories, one with three ablation locations and the other with a single ablation. The FRE was 1.2 mm, confirming that the 3-D image and patient space fiducials were acquired at approximately the same respiratory phase. No complication was observed during the procedure.

The second study was also successful. Following manual segmentation, automated planning was completed within 197 s. The prescribed plan consisted of two trajectories, each with a single ablation. The FRE for this study was 0.9 mm, confirming that the 3-D image and patient space fiducials were acquired at similar respiratory phases.

The third study was successful in terms of navigation but a failure from a survival standpoint. Automated planning was completed within 18 s. The prescribed plan consisted of two trajectories, each with a single ablation. FRE for this study was 0.5 mm, confirming that the 3-D image and patient space fiducials were acquired at the same respiratory phase. After the second ablation was performed, the animal died due to respiratory failure. Further pathological analysis showed that the animal had been suffering from mycoplasma pneumonia infection that caused fatal respiratory compromise.

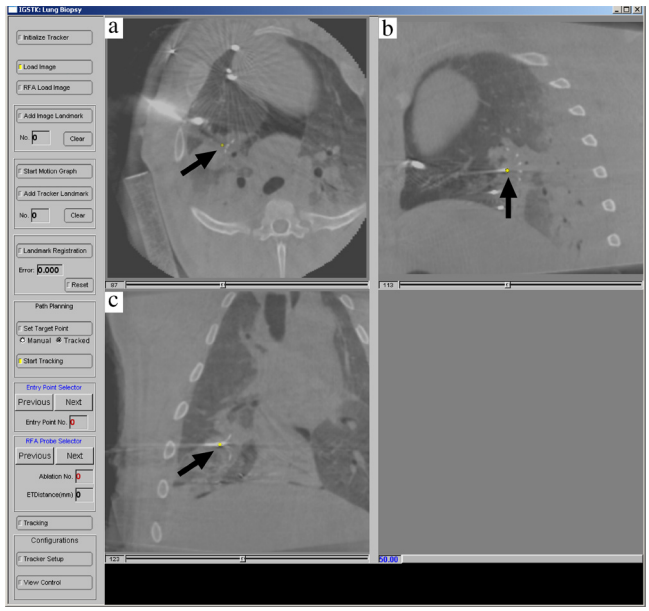

Fig. 10. Confirmation scan after RFA electrode insertion (a) axial, (b) sagittal, and (c) coronal views. Arrow points to tip of the probe, which was manually identified and marked.

The mean (std) navigation error estimate based on the registration between planning image and confirmation images was 11.6 (3.3) mm. Fig. 10 shows a sample confirmation scan.

It should be noted that the worst case running time of the planning phase is exponentially dependent on the number of tumor and entry points used as input which, in turn, depend on the size of the tumor and the grid spacing used for discretization. Based on input from our collaborating physicians, a computation time of less than 5 min is clinically acceptable. To reduce our running time, we are currently investigating the use of the simulated annealing optimization heuristic. We expect that this heuristic will improve our running times, although it does not guarantee that the solution will be obtained in less than 5 min.

C. *Lung Biopsy System*

The lung biopsy system was evaluated in an ongoing clinical trial at Georgetown University Hospital. The protocol for the interventions was limited to a single navigation session. That is, the system was used as described earlier, with a confirmation scan acquired once navigation was completed. If the needle tip was found to be inside the suspected lesion, a biopsy sample was acquired. If the needle was outside the lesion the procedure was completed using CT fluoroscopy for guidance.

The first clinical case was successful, confirmation image showed the needle tip inside the lesion (see Fig. 11). Patient was placed in the prone position and the targeted lesion was in the left lower lobe. The navigation error estimated based on the registration between planning image and confirmation

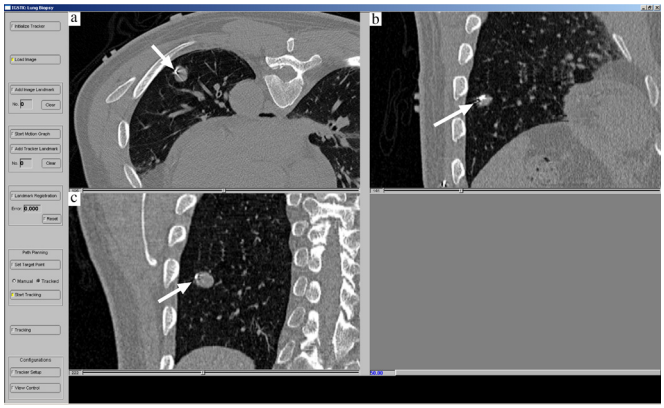

Fig. 11. Confirmation scan from first clinical case. (a) axial, (b) sagittal, and (c) coronal views. Arrow points to tip of the needle embedded in the suspected lesion.

image was 9.68 mm. No complication was observed during the procedure.

The second clinical case was partially successful, confirmation image showed the needle nearly inside the suspected lesion. The patient was in the prone position, and the targeted lesion was in the left upper lobe. A slight retraction of needle was sufficient to obtain a biopsy sample, without using additional CT-fluoroscopy guidance. The navigation error estimated based on the registration between planning image and confirmation image was 7.37 mm. No complication was observed during the procedure.

The third clinical case was considered a failure, confirmation image showed the needle outside the suspected lesion. Patient was placed in the prone position, and the targeted lesion was in the right lower lobe near the diaphragm. Additional adjustment of needle under CT fluoroscopy was required. The navigation error estimated based on the registration between planning image and confirmation image was 3.87 mm. Despite the smallest error of the three clinical cases, the biopsy did not yield a diagnostic specimen. Patient also experienced a small localized pneumothorax, that is the underlying target location had shifted during the procedure.

IV. Discussion and Conclusion

We have presented three systems for navigated needle interventions, including vertebroplasty, lung RFA of large tumors, and lung biopsies. The former system deals with a rigid anatomical structure, the spine, while the latter two deal with dynamically moving structures whose motion is influenced by the patient's respiration. To accommodate this motion physicians are expected to gate their actions to a stable respiratory phase, end expiration.

The vertebroplasty system was evaluated in a phantom study, enabling quantitative performance analysis of multiple users under the same conditions. From the experimental results, we observe that the three levels of expertise, student, fellow, and attending physician are reflected by the accuracy and procedure duration. All operators, irrespective of experience level, successfully completed the procedures. We thus conclude that our system can potentially reduce the radiation dose required to perform the procedure by a less experienced operator as it only requires a single CBCT acquisition at the beginning of the procedure. On the other hand, we have also seen that the system is not able to compensate for the lack of expertise in terms of accuracy and procedure duration.

The lung RFA system was evaluated in an approved animal survival study. All probe navigation passes were completed successfully. In one of the three studies the animal did not survive the intervention. Retrospective analysis of this case concluded that the animal had been suffering from pneumonia, which greatly reduced its chances of surviving the procedure. The mean accuracy of the RFA electrode placement was 11.6 mm. This is a significant error, which we attribute to several factors. The inherent inaccuracy of gating actions to the same respiratory phase as the one in which the 3-D image was acquired, the fact that the tip of the navigated stylet did not coincide with the tip of the RFA electrode, which is the point of interest, a difference of approximately 3 mm between the points, and the inherent accuracy limitations of electromagnetic tracking.

The lung biopsy system was used in three clinical cases. The use of CT fluoroscopy for navigation was reduced in all interventions, with no fluoroscopic imaging in two of the cases. For the third case, fluoroscopy was required to complete the procedure. In this case, the targeted lesion exhibited considerable motion due to its location next to the diaphragm. This location combined with the patient lying in the prone position reduced the accuracy of gating actions to the end-expiration phase. As a result, needle advances were not performed at the correct respiratory phase, invalidating our assumption of quasi-rigid structures. In addition, the underlying anatomy had changed, small pneumothorax, after image acquisition. Thus, the volumetric data we used provided a less accurate representation of the underlying anatomy.

The majority of the software components used in implementing the systems described in this work have been incorporated into the IGSTK. An example application, navigator, showcasing these capabilities is available for download from the toolkits Web site [28] and is intended to serve as a starting point for developers of image-guided navigation systems. Detailed descriptions of the various IGSTK components and how to use them in implementing a navigation system are given in [29]. This book is freely available in pdf format from http://www.igstk.org/IGSTK/help/documentation.html.

Based on our experience developing and evaluating the various systems, we have gained the following insights.

1) Real-time intraoperative imaging should be incorporated as part of the procedure to monitor possible changes in the underlying anatomical structures that cannot be detected by the navigation system (e.g., pneumothorax). This addresses an inherent feature of image-guided navigation systems, they are open-loop systems with the physician responsible for closing the loop either by occasional imaging or possibly, tactile feedback.
2) The quasi-rigid assumption and the user-gated advancement of tools is not sufficiently accurate for tumors that

exhibit considerable motion. In our case, tumors near the diaphragm.

3) An explicit plan should always be required. Specifying a plan in advance facilitates safer interventions by allowing the physician to gain a better understanding of the anatomical structures that will be pierced by the tool. This is increasingly important in the presence of abnormal anatomy. In addition, for cases in which there are complications it is easier to identify the cause. In such cases, problems can be traced either to a suboptimal plan or to problems executing the plan. This differs from current clinical practice, in all three procedures, where plans are not explicitly specified. Thus, there is no way to quantitatively compare the physician's intentions and the actual performance.

We are currently investigating the acquisition and use of 4-D (3-D+time) image data for image-guided interventions [30]. This approach will allow the patient to freely breath during image acquisition and will enable the physicians to advance tools without the need of gating their actions to a specific respiratory phase. We believe that this approach will result in a more streamlined workflow, and potentially, improved interventional accuracy.

APPENDIX

LUNG RFA PLANNING

To plan the RFA electrode insertion trajectories and ablation locations, we first discretize the data by superimposing a lattice with fixed spacing g onto the segmented images. Based on the clinical considerations described in the text mentioned earlier, the following set of optimization problems are formulated and solved.

Minimizing Number of Needle Trajectories

Our first objective is to determine the smallest set of needle trajectories needed to cover the lesion and its margin, given a particular pleural entry point. Given the set of trajectories TR, defined by the entry point and the set $T \cup M$, we seek the smallest subset of needle trajectories, which treats $T \cup M$. The cylindrical treatment volume covered by a series of overlapping ablation spheres of radius A along a trajectory consists of all points within a distance αA, $\alpha = \frac{1}{A}\sqrt{A^2 - (\frac{g}{2})^2}$, from the trajectory. Given this we define the following binary decision variables:

$$x_t = \begin{cases} 1, & \text{if trajectory } t \text{ is used} \\ 0, & \text{otherwise} \end{cases}$$

where $t \in TR$, the proposed set of trajectories. Our objective is thus to find the minimum number of trajectories TR^* by solving the optimization problem.

$$\min \sum_{t \in TR} x_t$$

$$\text{subject to} \sum_{t \in TR:\ d(c,t) \le A} x_t \ge 1, c \in T \cup M \qquad (1)$$

where $d(c,t)$ is the minimum distance from a point c to trajectory t. This formulation minimizes the number of trajectories while enforcing that every tumor and margin point is treated by at least one trajectory. This binary integer linear programming optimization is then solved using the branch and bound algorithm.

Minimizing Number of Ablations

Our next objective is to determine the minimal number of ablations given a specific set of trajectories. Given TR^* we now determine where to place ablations along the trajectories in this set of trajectories. We consider a set $D(TR^*)$ of potential ablation centers along the trajectories in TR^*, where initially, the ablation centers are chosen to be some fixed distance apart along the trajectory. We then define the binary decision variables

$$y_a = \begin{cases} 1, & \text{if an ablation is centered at } a \\ 0, & \text{otherwise} \end{cases}$$

for all potential ablation centers $a \in D$. We then formulate an integer program to find D^*, as

$$\min \sum_{a \in D(TR^*)} y_a$$

$$\text{subject to} \sum_{a \in D(TR^*):\|a-c\| \le A} y_a \ge 1, c \in T \cup M. \qquad (1)$$

This formulation minimizes the number of ablations while enforcing that every tumor and margin point is treated by at least one ablation. Moreover, in this formulation, it easy to incorporate the constraint of avoiding critical structures (NF and NP) by eliminating from the set any ablation center that touches a critical point. This optimization is solved using the branch and bound algorithm.

After determining the minimal number of ablation centers for a given set of trajectories, we select a new entry point from the set of potential entry points and repeat the two optimization steps described earlier, minimizing number of needle trajectories and minimizing number of ablations. After all potential entry points have been analyzed, we choose the one that has the smallest number of needle trajectories and least number of ablations, in that order. Following the identification of this solution, we employ a heuristic to minimize the damage to healthy tissue, as follows.

Minimizing Damage to Healthy Tissue

At this stage, we are left with a best strategy, where a strategy is a set of trajectories TR^* and the minimum set of ablation centers along those trajectories D^*. At this point, our final objective is to minimize the damage to healthy tissue. We point out that the goal of minimizing healthy tissue damage is equivalent to the goal of maximizing ablation *redundancy*—the more times a point in $T \cup M$ is treated by different ablations, the less damage is done to healthy tissue. To achieve this goal, we employ a local search heuristic. This heuristic consists of:

1) Selecting (at random) one of the trajectories $t \in TR^*$.
2) Generating a new trajectory t' by perturbing trajectory t by a random angle around its entry point.

3) Considering a new set of trajectories TR^+, where $TR^+ = TR^*/\{t\} \cup \{t'\}$ and then resolving step two, minimizing number of ablations. In particular, if we define K_c as the number of ablations treating tumor cell c and D^+ as the set of potential ablation centers along the *new* set of trajectories TR^+, then we need to solve the following maximization problem:

$$\begin{aligned} \max \quad & \sum_{c \in T \cup M} K_c \\ \text{subject to} \quad & \sum_{a \in D^+ : \|a-c\| \leq \alpha A} y_a \geq 1 + K_c, c \in T \cup M \\ & \sum_{a \in D^+} y_a \leq D^* \\ & K_c \in \{1, 2, \ldots\}. \end{aligned} \tag{3}$$

The solution is again obtained using the branch and bound method. Note that by construction the number of trajectories is kept constant and, in addition, the constraint $\sum_{a \in D^+} y_a \leq D^*$ ensures that the number of ablations will be at most as many as in the original D^*. Let K^* be the optimal solution to this problem.

4) If K^* improves on the previous solution, then we replace the set TR^* with TR^+ and repeat the heuristic search. This loop is executed a predetermined number of iterations.

Following completion of the heuristic to maximize ablation redundancy, we are left with an optimal treatment strategy that consists of a set of trajectories and ablation centers along each trajectory. The plan is optimal in that it ensures that the tumor and prescribed ablation margin are covered, while minimizing the amount of damage to healthy tissue and limiting the number of punctures to the pleura.

ACKNOWLEDGMENT

The authors would like to thank Dr. C. Golding, J. Ding, and N. Khan for their help in the evaluation of the vertebroplasty navigation system. They would also like to thank N. Glossop of Traxtal Technologies Inc., for supplying the MagTrax needles and tracked trocar used by the vertebroplasty and lung RF ablation navigation systems. The content of the manuscript does not necessarily reflect the position or policy of the U.S. Government.

REFERENCES

[1] T. Peters and K. Cleary, Eds., *Image-Guided Interventions Technology and Applications*. New York: Springer-Verlag, 2008.

[2] A. Enquobahrie, P. Cheng, K. Gary, L. Ibáñez, D. Gobbi, F. Lindseth, Z. Yaniv, S. Aylward, J. Jomier, and K. Cleary, "The image-guided surgery toolkit IGSTK: An open source C++ software toolkit," *J. Digital Imag.*, vol. 20, no. Suppl. 1, pp. 21–33, 2007.

[3] Z. Yaniv and K. Cleary, "Image-guided procedures: A review," Image Science and Information Systems Center, Georgetown Univ. Washington, DC,Tech. Rep. CAIMR TR-2006-3, Apr. 2006.

[4] A. W. Burton and E. Mendel, "Vertebroplasty and kyphoplasty," *Pain Physician*, vol. 6, no. 3, pp. 335–341, 2003.

[5] N. T. Fitousi, E. P. Efstathopoulos, H. B. Delis, S. Kottou, A. D. Kelekis, and G. S. Panayiotakis, "Patient and staff dosimetry in vertebroplasty," *Spine*, vol. 31, no. 23, pp. E884–E889, 2006.

[6] R. Harstall, P. F. Heini, R. L. Mini, and R. Orler, "Radiation exposure to the surgeon during fluoroscopically assisted percutaneous vertebroplasty: A prospective study," *Spine*, vol. 30, no. 16, pp. 1893–1898, 2005.

[7] K. Perisinakis, J. Damilakis, N. Theocharopoulos, G. Papadokostakis, A. Hadjipavlou, and N. Gourtsoyiannis, "Patient exposure and associated radiation risks from fluoroscopically guided vertebroplasty or kyphoplasty," *Radiology*, vol. 232, no. 3, pp. 701–707, 2004.

[8] S. C. Rose, "Radiofrequency ablation of pulmonary malignancies," *Semin. Respir. Crit. Care Med.*, vol. 29, no. 4, pp. 361–383, 2008.

[9] A. R. Gillams and W. R. Lees, "Radiofrequency ablation of lung metastases: Factors influencing success," *Eur. Radiol.*, vol. 18, no. 4, pp. 672–677, 2008.

[10] R. Lencioni, L. Crocetti, R. Cioni, R. Suh, D. Glenn, D. Regge, T. Helmberger, A. Gillams, A. Frilling, M. Ambrogi, C. Bartolozzi, and A. Mussi, "Response to radiofrequency ablation of pulmonary tumours: A prospective, intention-to-treat, multicentre clinical trial (the RAPTURE study)," *Lancet Oncol.*, vol. 9, no. 7, pp. 621–628, 2008.

[11] M.-H. Chen, W. Yang, K. Yan, M.-W. Zou, L. Solbiati, J.-B. Liu, and Y. Dai, "Large liver tumors: protocol for radiofrequency ablation and its clinical application in 110 patients—Mathematic model, overlapping mode, and electrode placement process," *Radiology*, vol. 232, no. 1, pp. 260–271, 2004.

[12] G. D. D. III, M. S. Frank, M. Aribandi, S. Chopra, and K. N. Chintapalli, "Radiofrequency thermal ablation: Computer analysis of the size of the thermal injury created by overlapping ablations," *Amer. J. Roentgenol.*, vol. 177, no. 4, pp. 777–782, 2001.

[13] C. Hohl, C. Suess, J. E. Wildberger, D. Honnef, M. Das, G. Muhlenbruch, A. Schaller, R. W. Gunther, and A. H. Mahnken, "Dose reduction during CT fluoroscopy: Phantom study of angular beam," *Radiology*, vol. 246, no. 2, pp. 519–525, 2008.

[14] B. M. Stoeckelhuber, T. Leibecke, E. Schulz, U. H. Melchert, C. U. Bergmann-Koester, T. Helmberger, and J. Gellissen, "Radiation dose to the radiologist's hand during continuous CT fluoroscopy-guided interventions," *Cardiovasc. Intervent. Radiol.*, vol. 28, no. 5, pp. 589–594, 2005.

[15] L. Mundeleer, D. Wikler, T. Leloup, and N. Warzée, "Development of a computer assisted system aimed at RFA liver surgery," *Comput. Med. Imag. Graph.*, vol. 32, no. 7, pp. 611–621, 2008.

[16] A. State, H. Yang, H. Fuchs, S. W. Lee, P. McNeillie, and C. Burke, "Contextually enhanced 3D visualization for multi-burn tumor ablation guidance," in *Proc. Workshop Augmented Environ. Med. Imag. Comput. Aided surg. (AMI-ARCS)*, 2008, pp. 70–77.

[17] S. Nicolau, X. Pennec, L. Soler, X. Buy, A. Gangi, N. Ayache, and J. Marescaux, "An augmented reality system for liver thermal ablation: Design and evaluation on clinical cases," *Med. Image Anal.*, vol. 13, no. 3, pp. 494–506, 2009.

[18] M. J. Wallace, M. D. Kuo, C. Glaiberman, C. A. Binkert, R. C. Orth, and G. Soulez, "Three-dimensional C-arm cone-beam CT: Applications in the interventional suite," *J. Vasc. Interv. Radiol.*, vol. 19, no. 6, pp. 799–813, 2008.

[19] W. Birkfellner, F. Watzinger, F. Wanschitz, R. Ewers, and H. Bergmann, "Calibration of tracking systems in a surgical environment," *IEEE Trans. Med. Imag.*, vol. 17, no. 5, pp. 737–742, Jun. 1998.

[20] Z. Yaniv, E. Wilson, D. Lindisch, and K. Cleary, "Electromagnetic tracking in the clinical environment," *Med. Phys.*, vol. 36, no. 3, pp. 876–892, 2009.

[21] X. Liu, H. Cevikalp, and J. M. Fitzpatrick, "Marker orientation in fiducial registration," in *Proc. SPIE Med. Imag.: Image Process.*, 2003, pp. 1176–1185.

[22] J. Ding, N. Khan, P. Cheng, E. Wilson, V. Watson, K. Cleary, and Z. Yaniv, "Accuracy analysis of an image-guided system for vertebroplasty therapy based on electromagnetic tracking of instruments," in *Proc. SPIE Med. Imag.: Vis., Image-Guided Procedures, Display*, 2008, pp. 69181K-1–69181K-7.

[23] B. K. P. Horn, "Closed-form solution of absolute orientation using unit quaternions," *J. Opt. Soc. Amer. A*, vol. 4, no. 4, pp. 629–642, Apr. 1987.

[24] P. A. Yushkevich, J. Piven, H. Cody Hazlett, R. Gimpel Smith, S. Ho, J. C. Gee, and G. Gerig, "User-guided 3D active contour segmentation of anatomical structures: Significantly improved efficiency and reliability," *Neuroimage*, vol. 31, no. 3, pp. 1116–1128, 2006.

[25] C. R. Maurer, Jr, J. M. Fitzpatrick, M. Y. Wang, R. L. Galloway, Jr, R. J. Maciunas, and G. S. Allen, "Registration of head volume images using implantable fiducial markers," *IEEE Trans. Med. Imag.*, vol. 16, no. 4, pp. 447–462, Aug. 1997.

[26] J. M. Fitzpatrick, "Fiducial registration error target registration error are uncorrelated," in *SPIE. Medical Imaging*: *Visualization, Image-Guided Procedures, and Modeling*, vol. 7261, no. 1, pp. 726102-1–726102-12, 2009.
[27] M. Tsuchida, Y. Yamato, T. Aoki, T. Watanabe, N. Koizumi, I. Emura, and J. Hayashi, "CT-guided agar marking for localization of nonpalpable peripheral pulmonary lesions," *Chest*, vol. 116, no. 1, pp. 139–143, 1999.
[28] The Image-Guided Surgery Toolkit. (2009). [Online]. Available: http://www.igstk.org
[29] K. Cleary, P. Cheng, A. Enquobahrie, and Z. Yaniv, Eds., *IGSTK: The Book*. Gaithersburg, MD: Signature Book Printing, 2009.
[30] A. Hartl and Z. Yaniv, "Evaluation of a 4D cone-beam CT reconstruction approach using a simulation framework," in *Proc. Int. Conf. IEEE Eng. Med. Biol. Soc. (EMBC)*, 2009, pp. 5729–5732.

Author's photographs and biographies not available at the time of publication.